Int. J. Electrochem. Sci., 8 **(2013)** 5396 - 5406

International Journal of
ELECTROCHEMICAL
SCIENCE
www.electrochemsci.org

Nickel-Modified and Zirconium-Modified Li_2MnO_3 and Applications in Lithium-Ion Battery

Bingjing Li[1,2], *Qibao Wang*[1,*], *Yong Zhang*[2], *Zhansong Song*[2], *Daming Yang*[2]

[1] China University of Mining & Technology, Beijing, 100083, PR China
[2] Mining Products Safety Approval and Certification Center, Beijing, 100013, PR China
[*]E-mail: wqb@cumtb.edu.cn

Received: 26 January 2013 / *Accepted:* 3 March 2013 / *Published:* 1 April 2013

Single-crystalline nanorods of monoclinic Li_2MnO_3 with about 200 nm in width and around 8 μm in length have been synthesized via a template-sintered reaction using γ-MnOOH nanorods as a template. Nickel-modified and Zirconium-modified Li_2MnO_3 cathode are also obtained respectively. Nickel-modified Li_2MnO_3 cathode ($0.5Li_2MnO_3 \cdot 0.5LiMn_{0.5}Ni_{0.5}O_2$) delivers the highest initial discharge capacity of 497 mAh/g at 0.1 C in the voltage range of 2.0-4.6 V. Although without distinct higher discharge capacity, Zirconium-modified Li_2MnO_3 cathode ($0.5Li_2MnO_3 \cdot 0.5LiMn_{0.5}Zr_{0.5}O_2$) improves cycle stability to a certain extent. Voltage plateaus of cathode materials can be apparently observed after modified by Nickel and Zirconium and electrochemical performance is enhanced.

Keywords: MnOOH; Li_2MnO_3; Cathode materials; Lithium-ion battery.

1. INTRODUCTION

Lithium-ion batteries (LIB) are considered as one of the most promising energy storage devices, not only for mobile electronics, but also for hybrid electric vehicle (HEV). Among the cathode materials, $LiCoO_2$ occupied most of market owning to the mature industrialization. However, it became the urgent point to develop substitutions due to expensive cost and gradual scarcity of Cobalt. A series of new materials were constantly reported, such as $LiNiO_2$, $LiMn_2O_4$, $LiMnO_2$ and $LiFePO_4$. But electrochemical properties should be further improved for extensive industrialization [1–4].

In recent years, the complicated compounds with the layered R-3m structure have been growing interested. It was respectively reported that $LiMn_{0.5}Ni_{0.5}O_2$ [5], $LiMn_{0.33}Ni_{0.33}Co_{0.33}O_2$ [6], and $LiNi_{1-x}Co_xO_2$ [7–9] were obtained to effectively improve structural integrity and enhance electrochemical performance. Monoclinic Li_2MnO_3 was also receiving worldwide attention due to high discharge capacity (250 mAh/g) at approximately 4.6 V vs. Li^+/Li [10, 11]. The close-packed composites $xLi_2MnO_3 \cdot (1-x)LiMO_2$ (M=Mn, Ni or Co) was investigated with integrated structure. The Li_2MnO_3 component supplying surplus lithium to the layered structure plays a critical role in stabilizing the electrode structure at low lithium loadings [12]. During the process of initial charge, lithium ions in the transition metal layers diffuse into the lithium-depleted layers to provide sufficient binding energy in order to maintain the integrity of the close-packed oxygen array [13,14], which enhanced the discharge capacity of the electrode.

Up to now, some gratifying results have been continuously reported recently. For instance, $0.3Li_2MnO_3 \cdot 0.7LiMn_{0.5}Ni_{0.5}O_2$ composite electrodes was investigated to deliver reversible capacity of 254 mAh/g, and the acid-treatment significantly improved the initial charge/discharge columbic efficiency [15]. The synthesis of $xLi_2MnO_3 \cdot (1\text{-}x)LiMn_{0.33}Ni_{0.33}Co_{0.33}O_2$ (x=0.5,0.7) was studied by the co-precipitation method followed heat treatment and elaborated the possible reasons for this anomalous high capacity[16]. Structurally integrated 'layered–layered' $xLi_2MnO_3 \cdot (1-x)LiMO_2$ cathode was synthesized with high Manganese content and further stabilized by NiO rock-salt regions, realizing the fabrication of high-capacity $xLi_2MnO_3 \cdot (1-x)LiMO_2$ with compositions close to the $LiMO_2$ apex on the Li_2MnO_3-$LiMO_2$ tie-line of a Li_2MnO_3-$LiMO_2$-MO_2 phase diagram [17]. Although some work has been reported and electrochemical performance has been more or less improved, there are many respects to enhance for application. It is necessary to engage much more research to develop high-performance $xLi_2MnO_3 \cdot (1-x)LiMO_2$ cathode materials.

Here we report the synthesis of Li_2MnO_3 and $0.5Li_2MnO_3 \cdot 0.5LiMn_{0.5}M_{0.5}O_2$ (M=Ni, Zr) by template-sintered process. Structure, morphology and electrochemical properties were thoroughly investigated by systemic testing and characterization. The influence caused by Nickel-modified and Zirconium-modified was detail demonstrated.

2. EXPERIMENTAL

γ-MnOOH nanorods was prepared by one-step hydrothermal method using $MnSO_4 \cdot H_2O$ and $KMnO_4$ as the starting materials. The stoichiometric amount of each material was mixed in distilled water. Then a required amount of CTAB (Hexadecyl trimethyl ammonium Bromide) was added as surfactant and stirred for an hour. Afterwards, the suspension was transferred into a 100 mL Teflon-lined stainless-steel autoclave, sealed and maintained at 160 ºC for 25 h. The product was cooled to room temperature, filtered and washed with distilled water, ethanol and acetone. The brown powder was obtained and dried under vacuum at 60 ºC for 10 h.

Pristine Li_2MnO_3 was prepared by the following procedure: A stoichiometrically required amount of as-prepared γ-MnOOH was added to an aqueous solution of $LiOH{\cdot}H_2O$ and stirred for an hour. A small excessive amount of $LiOH{\cdot}H_2O$ was used to make complete transformation of γ-MnOOH. The mixture was heated to dry then the solid product was ground and calcinated in air at 650 ºC for approximately 15 h.

The resulting Li_2MnO_3 nanorods (alternatively, $Li[Li_{1/3}Mn_{2/3}]O_2$) was treated with a 2 M HNO_3 solution at room temperature for 20 h to obtain a H^+ ion-exchanged product with approximate composition $H[Li_{1/3}Mn_{2/3}]O_2$ by chemically leaching lithium from Li_2MnO_3. Modified materials $0.5Li_2MnO_3{\cdot}0.5LiMn_{0.5}M_{0.5}O_2$ (M=Ni, Zr) were obtained as follows: A stoichiometric amount of as-prepared Li_2MnO_3 and respective nitrate were added in 0.1 M nitric acid and stirred overnight at room temperature. The solution was heated at 70 °C to dry. The solid product was ground and annealed at 450 °C for 6 h in air. For the synthesis of a layered–layered $0.5Li_2MnO_3{\cdot}0.5LiMn_{0.5}M_{0.5}O_2$ (M=Ni, Zr) composite structure, the overall reaction can be represented simply as: [17]

$$3Li_2MnO_3 + Ni(NO_3)_2 \rightarrow 4\{0.5Li_2MnO_3 \cdot 0.5LiMn_{0.5}Ni_{0.5}O_2\} + N_2O_5$$

The final products are respectively referred to as LMO-Ni and LMO-Zr in the following text.

X-ray diffraction (XRD, Rigaku D/Max-2400, Japan) using Cu Kα radiation was employed to identify the crystalline phase of the synthesized material. The data were recorded in the 10-80° 2θ range at the scanning rate of 6°/min. The patterns were analyzed by the Rietveld method as implemented in the program. Thermogravimetry (TG) was carried out in air using NETZSCH STA 449C. X-ray photoelectron spectroscopy (XPS) was collected using American PHI5700ESCA with a non-monochromatic Mg Kα (1253.6eV) light source. The C 1s XPS at 284.6eV was used as the calibration of the spectra. It is a very useful method for studying surface properties, providing chemical information such as the oxidation state, as well as the semi-quantitative composition of the surface. Scanning electron microscopy (SEM, Hitachi S-4800, Japan), transmission electron microscopy (TEM) and high-resolution transmission electron microscopy (HR-TEM, JEOL-2100F, Japan) were engaged to observe morphology, size and distribution of as-prepared composites.

The electrodes were fabricated by casting a slurry of 75 wt.% active material, 15 wt.% carbon black, and 10 wt.% poly(vinylidene fluoride) (PVDF) in *N*-methylpyrrolidinone (NMP) solvent onto an Al foil substrate. The slurry was dried in vacuum at 60 °C overnight. The film was cut into pieces of about 0.6×0.6 cm^2 to act as electrodes. The testing half-cells were assembled in an Ar-filled glove box (MB-10-G with TP170b/mono, MBRAUN) with lithium metal as counter and reference electrode. Electrolyte was 1M $LiPF_6$ in a mixed solution of EC and DEC (1:1 in volume ratio). The charge-discharge measurements were galvanostatically carried out using a battery test system (NEWARE BTS-610, Newware Technology Co., Ltd., China) at 0.1 C in the voltage range of 2.0-4.6V (vs. Li/Li^+).

3. RESULTS AND DISCUSSION

Figure 1 shows the TG curve of γ-MnOOH nanorods. There are two main weight loss steps in the temperature range of 150-330 ºC and 540-600 ºC, respectively. The former weight loss (about 5.85%) is due to the decomposition of γ-MnOOH into β-MnO_2, higher than the calculated value (around 1.20%). It could attribute to the decomposition of the residual CTAB, which is entirely decomposed at 250 ºC. The latter (about 7.15%) contributes to the further transformation from β-MnO_2 to α-Mn_2O_3, consistent with the theoretical value. No weight loss can be observed over 600 ºC. The results are similar to the works previously reported [19, 20]. In this work, the temperature of synthesis can be described as follows:

$$4\gamma - MnOOH(s) + O_2(g) \xrightarrow{300^{\circ}C} 4\beta - MnO_2(s) + 2H_2O(g) \quad (1)$$

$$\beta - MnO_2(s) + 2\,LiOH(s) \xrightarrow{650^{\circ}C} Li_2MnO_3(s) + H_2O(g) \quad (2)$$

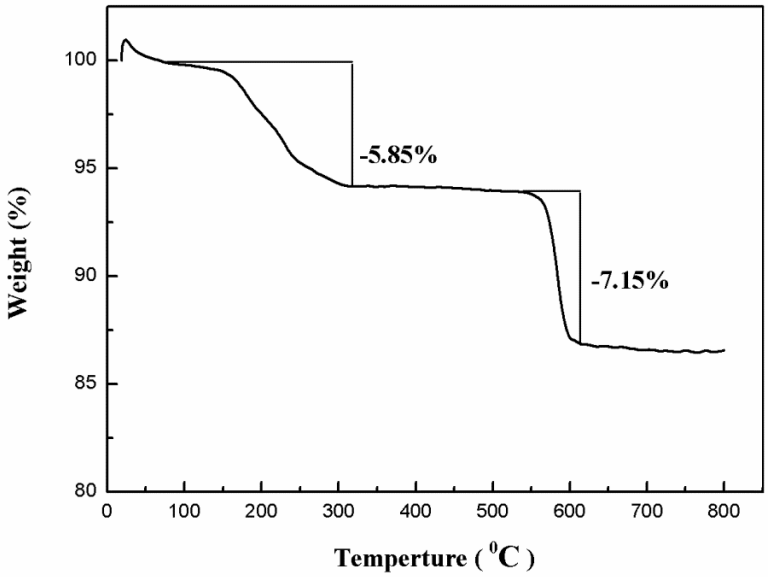

Figure 1. TG curve of the as-synthesized γ-MnOOH nanorods.

Figure 2a shows Rietveld refinement pattern of γ-MnOOH indexed to a monoclinic phase (JCPDS No.41-1379) with lattice constants a=5.300Å, b=5.278Å and c=5.307Å. No impurity phases can be observed, indicating the high purity of the products. Fig.2b shows the SEM image of the as-prepared γ-MnOOH nanorods. It is can be observed that large quantity of uniform rod-like nanostructures with about 200-300 nm in width and approximately 8 μm in length. The rod-like

nanostructure of the sample is further examined by TEM and HRTEM, respectively shown in Fig.2c-2e. It indicates its single-crystalline structure, corresponding selected area electron diffraction (SAED) pattern (Fig.2d). The diffraction spots can be indexed to $(11\bar{1})$, (020) and $(1\bar{3}1)$ planes of monoclinic γ-MnOOH (JCPDS No.41-1379). The HRTEM image (Fig.2e) corresponding to the circled area marked in Fig.2c indicates clearly the atom arrangements, which further confirms the single-crystalline structure of γ-MnOOH. As depicted in Fig.2e, interplanar spacings of (020) and $(11\bar{1})$ are 2.6 Å and 3.4Å, respectively.

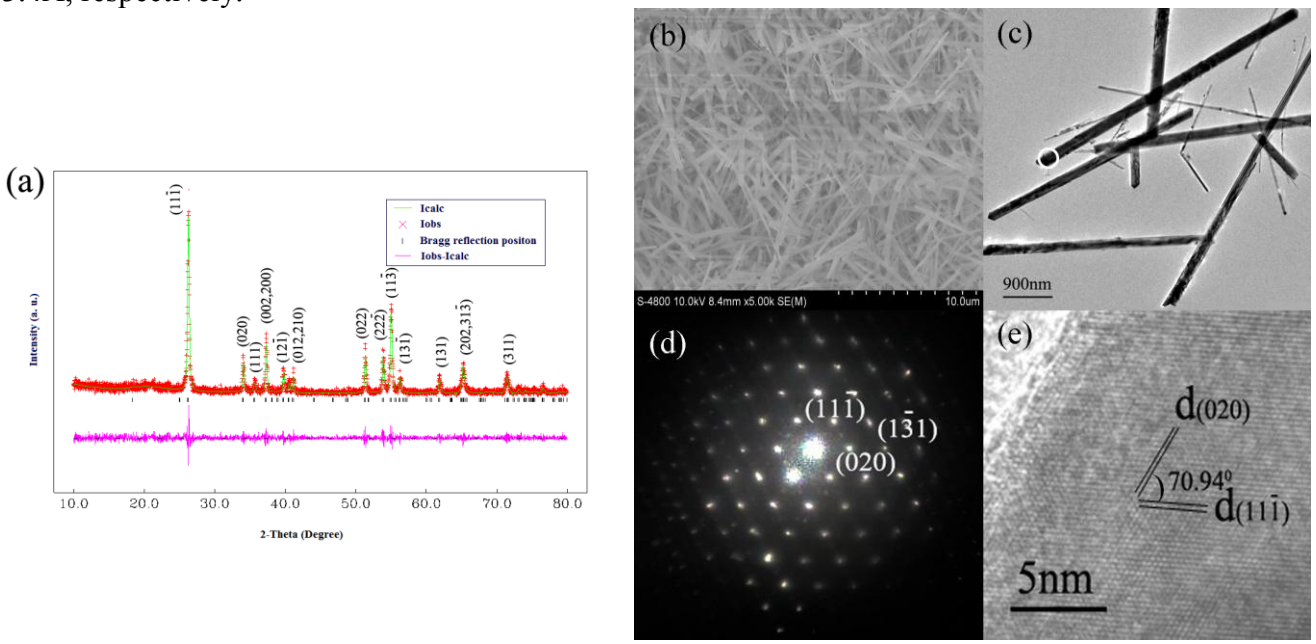

Figure 2. (a) Rietveld refinement pattern of γ-MnOOH nanorods; (b) SEM, (c) TEM, (d) corresponding SAED patterns and (e) HR-TEM images of γ-MnOOH nanorods.

Figure 3 shows the XRD patterns of Li_2MnO_3, acid-treated Li_2MnO_3, LMO-Ni and LMO-Zr. It can be indexed as a Li_2MnO_3 monoclinic structure with a space group of C2/m, the same as that of R3m layered rock-salt structures, as shown in Fig.3a. It was evident that the low-intensity ordering peaks at 2θ degree of 21-23° (arrowed in Fig.2b-d) was the characteristic of a Li_2MnO_3-type structure with $LiMn_6$ (or Ni-substituted) cation arrangements in the transition metal layers [21, 22]. The XRD pattern of acid-treated Li_2MnO_3 (Fig.3b) displays representative of an ion-exchanged product with nominal composition $H[Li_{1/3}Mn_{2/3}]O_2$. The slight shift of the peaks, the collapse of the peak at 2θ=44°-45°, and the retention of the broad but weak peaks at 2θ=21–23° are consistent with the shearing of the oxygen planes from O3 to P2 stacking and the maintenance of Li-Mn ordering in the Mn-rich layers [23]. Although impurity peaks (ZrO_2) are maintained in Fig.2c, it may play a role in stable structure during the process of charge and discharge due to electrochemical inactivity of ZrO_2. A major advantage of two-component $xLi_2MnO_3 \cdot (1-x)LiMO_2$ notation to describe the composition of complex layered electrodes containing lithium in the transition metal (M) layers, instead of the equivalent

layered notation $Li[Li_{x/(2+x)}Mn_{(1+x)/(2+x)}M_{(1-x)/(2+x)}]O_2$, it is easy to follow the changes in the overall composition of the electrodes during charge and discharge on a Li_2MnO_3–MO_2–$LiMO_2$–Li_2MO_2 phase diagram [15].

Figure 4 shows the XPS results of LMO-Ni and LMO-Zr. The binding energy of Mn $2p_{3/2}$ (Fig.4b and 4d) of samples are both about 642.5eV, agreement with preceding report for MnO_2 (Galakhov et al., 2000), indicating that the predominant Mn species near the surface is Mn (IV). The Ni $2p_{3/2}$ peak (Fig.5a) at 852.3eV is close to the over lapping peaks reported previously for $Ni(OH)_2$ and Ni_2O_3 (Oswald & Brückner, 2004).

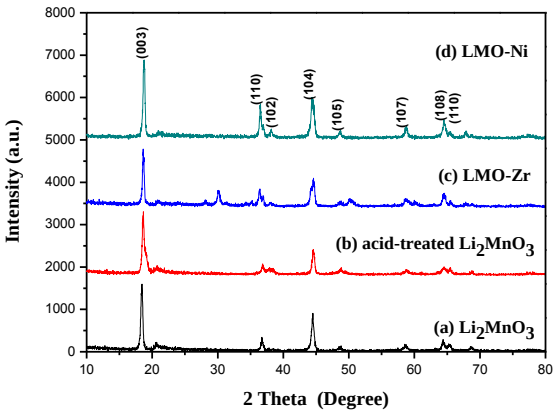

Figure 3. XRD patterns of a) Li_2MnO_3, b) acid-treated Li_2MnO_3, c) LMO-Ni, and d) LMO-Zr.

The Zr 3d peaks (Fig.4c) at 182.0eV and 179.5eV are respectively consistent to the research (Sarma & Rao, 1980) for Zr $3d_{3/2}$ and Zr $3d_{5/2}$. The $Zr3d_{3/2}$ at 182.0eV suggested the LMO-Zr contained Zr (IV) in ZrO_2, identical to the XRD results (Fig.2c).

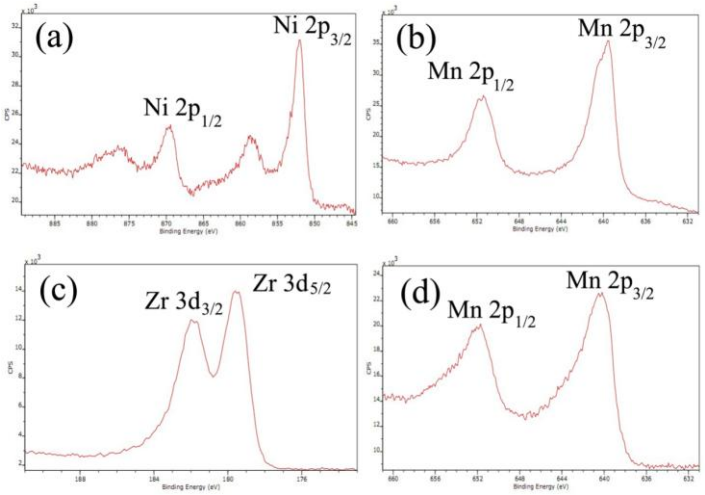

Figure 4. XPS patterns of LMO-Ni (a, b) and LMO-Zr (c, d).

Figure 5 shows SEM images of Li_2MnO_3, LMO-Ni and LMO-Zr, as well as TEM and SAED images of Li_2MnO_3. Rod-like nanostructure Li_2MnO_3 is about 300-400 nm in width and 8 μm in length, basically maintaining morphology of the precursor γ-MnOOH, as shown in Fig.5a. It can be observed that the thickness of nanorods is uniform and monoclinic Li_2MnO_3 is single-crystalline structure from TEM and SAED images (Fig.5b). Apparently, in situ formed LMO-Ni and LMO-Zr are still rod-like nanostructure, but shorter in length (Fig.5c and 5d). It is benefit to shorten the path for intercalation/deintercalation of lithium ion.

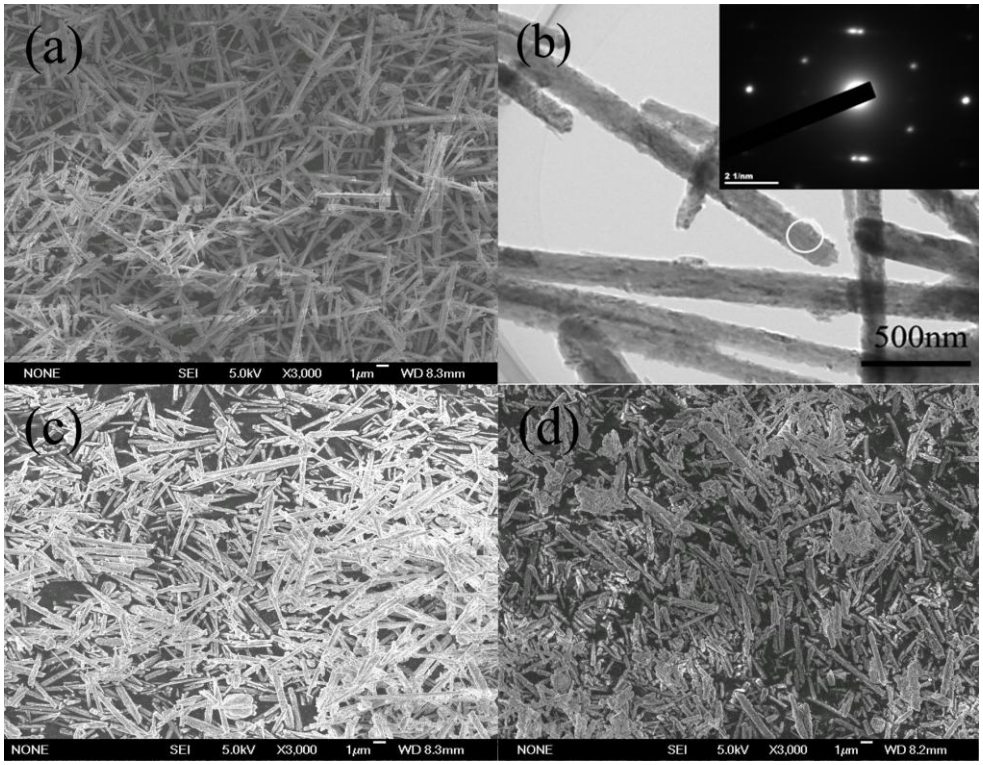

Figure 5. SEM images of (a) Li_2MnO_3, (c) LMO-Ni, and (d)LiMO-Zr, (b) TEM image of the Li_2MnO_3 nanorods, (insets) corresponding SAED patterns.

Figure 6 shows the initial discharge curves for the electrodes made from Li_2MnO_3, LMO-Ni and LMO-Zr. LMO-Ni sample has the largest initial discharge capacity (497 mAh/g). However, there is considerable excess of the theoretically expected values, probably contributing to side reactions involving electrolyte oxidation and proton generation [24, 25]. By contrast, Li_2MnO_3-Zr sample delivers the smallest initial discharge capacity (only 134 mAh/g), and pristine Li_2MnO_3 delivers 171 mAh/g. The initial discharge capacity for a plateaus around 2.8 V were observed for two modified samples, indicating a phase transition from $LiMn_{0.5}M_{0.5}O_2$ (M=Zr, Ni) to spinel phase caused by Li intercalation respectively on tetrahedral site and octahedral site [26]. It is obvious that the plateau length of LMO-Ni sample is longer than that of LMO-Zr. However, there is not distinct discharge

plateau in pristine Li_2MnO_3. It is suggested that electrochemical performance has been effectively improved through Nickel and Zirconium modified.

Figure 7 shows charge and discharge curves of 2nd, 5th, 10th and 20th cycles for Li_2MnO_3, LMO-Ni and LMO-Zr samples. Obvious discipline cannot be obtained for capacity, the height and length of plateaus in different cycles. It maybe attributes to sophisticated and ambiguous electrochemical reaction mechanism. Voltage plateaus during the process of charge and discharge for pristine sample is still not observed (Fig.7a). Both modified samples exhibit distinct charge and discharge plateaus (Fig.7b and 7c). The plateaus voltage of Zr-modified sample is a little higher than that of Ni-modified sample. As is all known, with plateaus of voltage is the foremost condition for the electrode materials to realize industrialization. Obviously, in spite of the capacity enhanced in varying degree after Nickel and Zirconium modified, the electrochemical performance of cathode materials has been thoroughly improved.

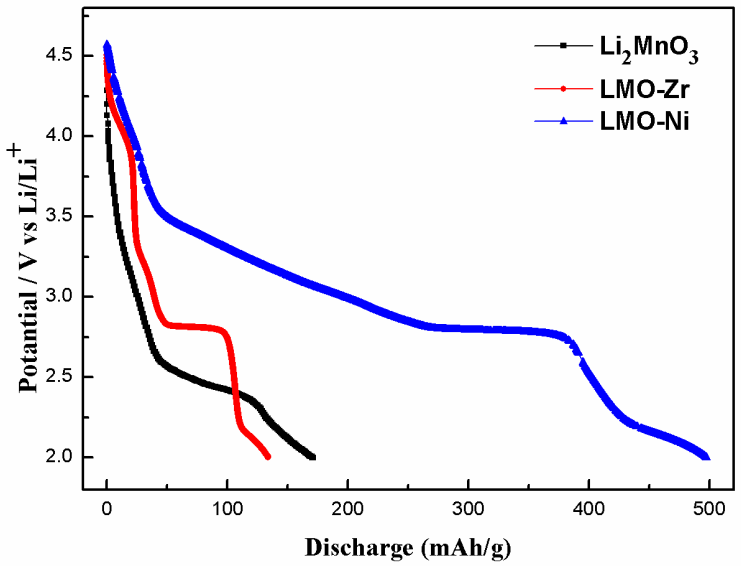

Figure 6. Initial discharge profiles for the electrodes made from Li_2MnO_3, LMO-Ni and LMO-Zr.

Figure 8 displays cycling stability of Li_2MnO_3, LMO-Ni and LMO-Zr samples for 20 cycles. The discharge capacity of LMO-Ni is much higher than any other samples, still retaining 220 mAh/g after 20 cycles, except the irreversible capacity loss on the initial cycle. Pristine sample has the irreversible capacity loss on the initial cycle. From 2nd cycle, the discharge capacity is gradually increasing, but still smaller than two modified samples. Although the initial discharge capacity for LMO-Zr is only 134 mAh/g, the irreversible capacity loss is 8 mAh/g and the capacity retention is 96%

after 20 cycles. It is probably due to Zr-O bond energy is stronger than Mn-O and Ni-O, in addition to a little amount of electrochemical inactive ZrO_2.

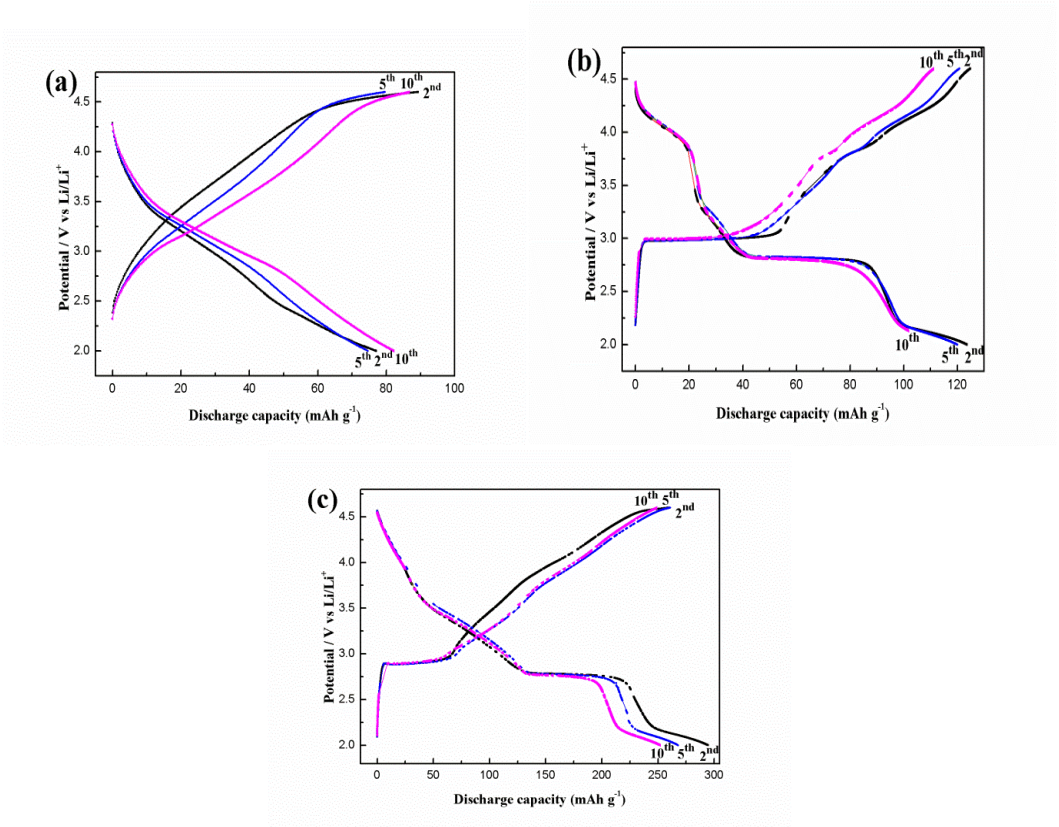

Figure 7. Charge and discharge curves of (a) Li_2MnO_3, (b) LMO-Zr and (c) LMO-Ni at 0.1 C in the range of 2.0-4.6 V.

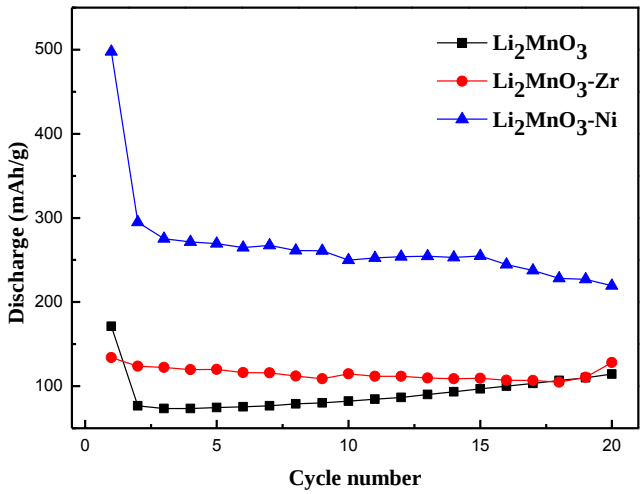

Figure 8. The cycle stability curves of the Li_2MnO_3, LMO-Zr and LMO-Ni at 0.1 C in the range of 2.0-4.6 V.

4. CONCLUSIONS

Pristine, Nickel-modified and Zirconium-modified Li_2MnO_3 samples have been synthesized and thoroughly investigated. The results show that Nickel-modified sample exhibits highest discharge specific capacity and the initial discharge capacity achieves 497 mAh/g. Zirconium-modified sample shows least irreversible loss. It makes cathode materials appear obvious charge and discharge plateaus after modifying. The electrochemical performance has been enhanced and the kinds of cathode materials become much more valuable in application.

ACKNOWLEDGEMENTS
This work was supported by the National Science & Technology Pillar Program (2012BAK04B09).

References

1. S.P. Sheu, C.Y. Yao, J.M. Chen, Y.C. Chiou, *J. Power Sources* 68 (1997) 533.
2. S.P. Sheu, I.C. Shih, C.Y. Yao, J.M. Chen, W.M. Hurng, *J. Power Sources* 68 (1997) 558.
3. S.S. Zhang, T.R. Jow, *J. Power Sources* 109 (2002) 172.
4. Y.-H. Huang, K.-S. Park, J.B. Goodenough, *J. Electrochem. Soc.* 153 (2006) A2282.
5. T. Ohzuku, Y. Makimura, *Chem. Lett.* 8 (2001) 744.
6. N. Yabuuchi, T. Ohzuku, *J. Power Sources* 119 (2003) 171.
7. A. Lecerf, M. Broussely, J.P. Gabano, *EP patent no.0345707, US patent no. 4980080* (1989).
8. T. Ohzuku, H. Komori, K. Sawai, T. Hirai, *Chem. Express 5* (1990) 733.
9. M. Balasubramanian, X. Sun, X.Q. Yang, J. McBreen, *J. Electrochem. Soc.* 147 (2000) 2903.
10. B.L. Ellis, K.T. Lee, L.F. Nazar, *Chem. Mater.* 22 (2010) 691.
11. J.-S. Kim, C.S. Johnson, J.T. Vaughey, M.M. Thackeray, S.A. Hackney, W. Yoon, C.P. Grey, *Chem. Mater.* 16 (2004) 1996.
12. M.M. Thackeray, C.S. Johnson, J.T. Vaughey, N. Li, S.A. Hackney, *J. Mater. Chem.* 15 (2005) 2257.
13. C.P. Grey, W.-S. Yoon, J. Reed, G. Ceder, *Electrochem. Solid-State Lett.* 7 (2004) A290.
14. K. Kang, G. Ceder, *Phys. Rev. B* 74 (2006) 094105-1.
15. C.S. Johnson, J.-S. Kim, C. Lefief, N. Li, J.T. Vaughey, M.M. Thackeray, *Electrochem. Commun.* 6 (2004) 1085.
16. C.S. Johnson, N. Li, C. Lefief, M.M. Thackeray, *Electrochem. Commun.* 9 (2007) 787.
17. J.R. Croy, S.-H. Kang, M. Balasubramanian, M.M. Thackeray, *Electrochem. Commun.* 13 (2011) 1063.
18. W.X. Zhang, Y. Liu, Z. Yang, S.P. Tang, M. Chen, *Solid State Commun.* 131 (2004) 441.
19. Z.H. Yang, Y.C. Zhang, W.X. Zhang, X. Wang, Y.T. Qian, X.G. Wen, S.H. Yang, *J. Solid State Chem.* 179 (2006) 679.
20. W.X. Zhang, Z.H. Yang, X. Wang, Y.C. Zhang, X.G. Wen, S.H. Yang, *Catal. Commun.* 7 (2006) 408.
21. P. Strobel, B. Lambertandron, *J. Solid State Chem.* 75 (1988) 90.
22. J. Bregér, M. Jiang, N. Dupre, Y.S. Meng, Y. Shao-Horn, G. Ceder, C.P. Grey, *J. Solid State Chem.* 178 (2005) 2575.
23. Y. Paik, C.P. Grey, C.S. Johnson, J.-S. Kim, M.M. Thackeray, *Chem. Mater.* 14 (2002) 5109.

24. A.D. Robertson, P.G. Bruce, Electrochem. *Solid-State Lett.* 7 (2004) A294.
25. M. Moshkovich, M. Cojocaru, H.E. Gottlieb, D. Aurbach, *J. Electroanal. Chem.* 497 (2001) 84.
26. P.G. Bruce, A.R. Armstrong, R.L. Gitzendanner, *J. Mater. Chem.* 9 (1999) 193.